Commun. Comput. Phys.
doi: 10.4208/cicp.071210.240511a

Vol. **11**, No. 3, pp. 709-725
March 2012

How the Antimicrobial Peptides Kill Bacteria: Computational Physics Insights

Licui Chen[1], Lianghui Gao[1,*], Weihai Fang[1] and Leonardo Golubovic[2]

[1] *College of Chemistry, Beijing Normal University, Beijing 100875, China.*
[2] *Physics Department, West Virginia University, Morgantown, West Virginia 26506-6315, USA.*

Received 7 December 2010; Accepted (in revised version) 24 May 2011

Available online 28 October 2011

Abstract. In the present article, coarse grained Dissipative Particle Dynamics simulation with implementation of electrostatic interactions is developed in constant pressure and surface tension ensemble to elucidate how the antimicrobial peptide molecules affect bilayer cell membrane structure and kill bacteria. We find that peptides with different chemical-physical properties exhibit different membrane obstructing mechanisms. Peptide molecules can destroy vital functions of the affected bacteria by translocating across their membranes via worm-holes, or by associating with membrane lipids to form hydrophilic cores trapped inside the hydrophobic domain of the membranes. In the latter model, the affected membranes are strongly buckled, in accord with very recent experimental observations [G. E. Fantner *et al.*, Nat. Nanotech., 5 (2010), pp. 280-285].

PACS: 87.15.-v, 82.70.Uv, 87.15.kt, 87.15.A-

Key words: Antimicrobial peptide, bilayer membrane, dissipative particle dynamics.

1 Introduction

Lipid bilayer membranes consisting of zwitterionic or acidic lipids are the essential components of cells and their organelles. They play very important roles in the living cells [1]: They can protect cell interior from the outside world; They can also interact with proteins and peptides to control the transport of substances into the cell and determine the metabolism of cells [2]. Antimicrobial peptides (AmPs) are bio-molecules employed by plants and animals for their defense against bacteria [3, 4]. These short chain peptides secreted by organisms are typically composed of 12-45 amino acid residues that carry

*Corresponding author. *Email address:* lhgao@bnu.edu.cn (L. Gao)

positive charges. When binding onto the outermost leaflet of negatively charged bacteria membrane by the aid of hydrophobic and electrostatic interactions, the antimicrobial peptides fold to amphipathic secondary structures, typically α-helices and β-sheets. Such peptides can kill the bacteria via either physical, chemical, or biological processes.

The vital function of the AmPs attracts both experimental and theoretical interest to elucidate their still elusive killing mechanisms. An appealing picture of this process was provided by the phenomenological Shai-Matsuzaki-Huang (SMH) model [5–7] which suggests that the peptides kill the cell by inserting into bacterial membrane to create holes that cause cellular content to leak out: When the peptides bind onto the surface of membrane, they displace the lipids and alter the membrane structure by thinning the bilayer and increasing the local surface tension of the bilayer. When the surface tension increases over a threshold value, the bilayer will rupture and permit the peptides permeate into the interior of the target cell. According to the structure of the insertion state, a number of models are suggested, such as "barrel-stave model", "carpet model", and "toroidal-pore model".

Many theoretical and numerical methods have also been used to study the molecular mechanism of the cell lysis by antimicrobial peptides, such as molecular- mean-field theory [8], all-atom molecular dynamics simulations [9–12], and coarse-grained simulations [13–17]. Most of these approaches support the SMH model that a physical hole in the membrane is stable and is an effective mechanism of antimicrobial activity.

In our recent paper [18], we reported a numerical study of the dynamic processes of cationic antimicrobial peptide translocation across a lipid bilayer membrane composed of both zwitterionic phospholipids and acidic phospholipids. Our study employed dissipative particle dynamics (DPD) simulations [19–21] in which both solvent and counterions are included explicitly. The advantage of the DPD method is that it allows simulations of large system in long time such that the full process of the peptide transport across the membrane becomes observable. Our study [18] also supports the SMH model, that the peptide can translocate across the bilayer membrane via a transmembrane hole. But the intermediate metastable peptide insertion state is composed of only one peptide. We also found that there are two mechanisms for peptide translocation: local tension increase and electrostatic attraction. Via electrostatic attraction, the peptide translocation is more reliable and, moreover, can occur at relatively low peptide concentrations.

In this article, first we give a review on how to apply DPD simulations to study the antimicrobial peptide-bilayer membrane interactions. Then we further develop the DPD simulation into constant particle number, surface tension, normal pressure, and temperature ($N\gamma_s P_\perp T$) ensemble [22, 23]. The NPT ensemble is usually more physically relevant ensemble than the NVT (constant volume) ensemble. By modifying the interaction strength between peptides and lipids as well as interactions between peptides and water, we investigate the effects of various physical-chemical properties of the peptide on the membrane obstructing mechanism. We find that besides creating metastable physical holes, the peptides can obstruct the integrity of the membrane by forming a hydrophilic core trapped inside the hydrophobic domain of the membrane. This novel structure is

mainly composed of peptides and lipids from the outermost membrane leaflet. The hydrophilic core structure is much like that of the inner shell of a vesicle. The presence of the core induces strong curvature effects and local stresses acting on the nearby leaflets of the bilayer, which undergoes a significant corrugation (buckling deformation). Such striking effects of AmPs on bacteria cell membranes have been indeed seen in very recent experiments with antimicrobial peptides [27]. These effects are prone to destroy the integrity of the membrane and cause the loss of the vital function of the cell.

The paper is organized as follows. In Section 2, we introduce the DPD simulation method. We explain how to set the coarse-grained model, how to deal with the electrostatic interactions and the corresponding self-energy term, and we describe the algorithms used in Nγ_sP$_\perp$T ensemble. In Section 3, we give the simulation results and discuss the effects of various factors on the killing mechanism of the peptides. A conclusion is given in Section 4.

2 Model and simulation method

2.1 Dissipative particle dynamics

In DPD simulations, the elementary units are soft beads composed of several atoms or molecules. All the beads are assumed to have the same mass m_0 and diameter r_0 and interact via short-ranged effective forces. The time evolution of all the beads is governed by Newton's equation of motion. Therefore, at every time step, the set of positions and velocities, $(\mathbf{r}_i,\mathbf{v}_i)$, follows from the positions and velocities at earlier time. For particle i at position $\mathbf{r}_i$ and with momentum p_i, the total force on it is [20]

$$\mathbf{f}_i=\sum_{j\neq i}(\mathbf{F}^C_{ij}+\mathbf{F}^D_{ij}+\mathbf{F}^R_{ij}). \tag{2.1}$$

Here $\mathbf{F}^C_{ij}$ is a conservative force exerted on the particle i by the particle j,

$$\mathbf{F}^C_{ij}=a_{ij}(1-r_{ij}/r_0)\hat{\mathbf{r}}_{ij}, \tag{2.2}$$

with a_{ij} (in unit of k_BT/r_0) the maximum repulsion between i and j. In Eq. (2.1), the dissipative force $\mathbf{F}^D_{ij}$ and the random force $\mathbf{F}^R_{ij}$ have the forms

$$\mathbf{F}^D_{ij}=-\gamma_{ij}(1-r_{ij}/r_0)^2(\hat{\mathbf{r}}_{ij}\cdot\mathbf{v}_{ij})\hat{\mathbf{r}}_{ij} \tag{2.3}$$

and

$$\mathbf{F}^R_{ij}=\sqrt{2\gamma_{ij}k_BT}(1-r_{ij}/r_0)\zeta_{ij}\hat{\mathbf{r}}_{ij}, \tag{2.4}$$

where γ_{ij} (in unit of k_BTm_0/r_0^2) are the friction coefficients and ζ_{ij} are uniformly distributed random numbers. Above, the vectors $\mathbf{v}_{ij}\equiv\mathbf{v}_i-\mathbf{v}_j$ are the velocity differences between particles i and j, and r_0 is the cutoff of the interaction, above which all the interactions are zero.

Our model system is built up from seven types of beads: they are water beads, labeled by w; hydrophilic lipid head beads, labeled by h; hydrophilic peptide beads, labeled by ph; hydrophobic lipid tail beads, labeled by c; hydrophobic peptide beads, labeled by pc; lipid counterions, and peptide counterions. Each of the beads represents a group of real atoms, for example, the water is modeled as a single bead representing three water molecules. The lipid molecule has 11 beads with three of them being hydrophilic head beads connected in a chain. The remaining eight lipid beads form two hydrophobic chains each with four hydrocarbon beads that are attached to two adjacent head beads. The lipid bilayer membrane is composed of zwitterionic and acidic lipid molecules. For zwitterionic lipid, the lipid beads carry zero charge. For acidic lipid, one of the three head beads has a net negative charge $=-e$. Peptide is modeled as a bundle of four chains each consisting of seven beads connected in a string. Two adjacent chains are hydrophilic and charged with net positive charge $=+3e$; the other two chains are hydrophobic. For lipids or peptides, two adjacent beads are connected via harmonic spring potential

$$U_2(i,i+1)=\frac{1}{2}k_2(\mathbf{r}_{i,i+1}-l_0)^2, \tag{2.5}$$

where k_2 is the spring constant, l_0 is the unstretched length. The chain stiffness is described by a three-body potential

$$U_3=k_3[1-\cos(\phi)], \tag{2.6}$$

where k_3 is the bending constant, ϕ is the angle between the two bonds connecting beads i, j and k. In our system, counterions are included. Each counterion has a positive charge $=+e$ (for lipid counterions) or negative charge $=-e$ (for peptide counterions). The force parameters are as same as that used in [18], except in several cases where peptide-lipid and peptide-water interactions are modified as discussed in the Section 3.

2.2 Electrostatic interactions

Most of the antimicrobial peptides and bacterial membranes are charged, so the long range electrostatic interaction must be incorporated carefully. To avoid strong ion pairing of the soft beads in DPD simulations, Coulomb's law can not be used directly. Groot introduced a lattice sum method [24] where all the charges are spread out over the lattice nodes via a charge distribution function

$$f(r)=\frac{3}{\pi R_e^3}\left(1-\frac{r}{R_e}\right), \quad \text{for } r<R_e, \tag{2.7}$$

where R_e is the electrostatics smearing radius, with $R_e=1.6r_0$ employed in the present simulations. Then the averaged local charge density is obtained as,

$$\bar{\rho}_e(\mathbf{r})=\int f(\mathbf{r}-\mathbf{r}')\rho_e(\mathbf{r}')d^3\mathbf{r}'. \tag{2.8}$$

In practice, the charge assigned to each of the nodes is proportional to $1-r/R_e$. So the normalized charge distribution function is

$$f_i(\mathbf{r}_c)=\frac{1-|\mathbf{r}_i-\mathbf{r}_c|/R_e}{\sum_{i'}1-|\mathbf{r}_{i'}-\mathbf{r}_c|/R_e}, \tag{2.9}$$

which guarantees that the sum of all these charges on the nodes equals to the charge on the assigning bead. In Eq. (2.9), $\mathbf{r}_i$ is the position of node, $\mathbf{r}_c$ is the position of the ion. The sum runs over all nodes within a radius R_e from $\mathbf{r}_c$. Then a real-space successive overdamped relaxation method is used to solve the field equations, that is, the field is updated via the iteration

$$\psi(\mathbf{r}_i)=\psi(\mathbf{r}_i)+\zeta[\Gamma\bar{\rho}_e(\mathbf{r}_i)+\nabla\cdot(P(\mathbf{r}_i)\nabla\psi(\mathbf{r}_i))]. \tag{2.10}$$

Here $\zeta=0.15$ is analogous to a friction factor. In Eq. (2.10), $\Gamma=e^2/k_BT\varepsilon r_0=9.615$ (at room temperature) is a coupling constant which is independent of position. Here, the dielectric constant is that of water (with the relative permittivity $\varepsilon_r=78.3$ at room temperature). In Eq. (2.10), the $\mathrm{P}(\mathbf{r})=\langle p_i\rangle$ is the polarizability relative to pure water, with the average running over all the particles in a cell near $\mathbf{r}$. The p_i is the polarizability of particle i, which is 1 for water beads, head beads of lipids, hydrophilic beads of peptides, and all counterions, whereas it is 0.025 for the hydrocarbon beads of lipids and the hydrophobic beads of the peptides. Therefore, we get the reduced electrostatic potential energy in the form

$$U_{el}=\sum_{q_c}\sum_{i}q_c\psi(\mathbf{r}_i)f_i(\mathbf{r}_c), \tag{2.11}$$

where the sum runs over all the ions and the nodes inside the smearing radius of each ion.

2.3 Self energy

The lattice sum method for the electrostatic interactions introduced by Groot did not address the issue of self-energy that a charge is experiencing from its own charge distribution. This artifact results in a strong inward pressure [25]. Thus, a special care must be taken to subtract the virial contributed by the self-energy term, especially for the NPT ensemble. Recently we derived the general expression for the self-energy and corresponding virial terms for electrostatic interactions in dissipative particle dynamics simulations [26]. These important results are used in the simulations in Section 3, so we briefly outline them here.

If a charge distribution function is continuum as given by Eq. (2.7), the self-energy of the charge is

$$U_{self}^{q_c}=\frac{q_c^2}{4\pi\varepsilon_0 R_e}, \tag{2.12}$$

which is independent of the coordinate of the particle. Thus it has no contribution to the virial and force on the charge. Whereas, if we spread a charge out on the nodes of discrete lattice, the self-energy has the similar form to Eq. (2.11),

$$U_{self}^{q_c}=\sum_i q_c\psi_{self}^{q_c}(\mathbf{r}_i)f_i(\mathbf{r}_c). \tag{2.13}$$

This expression [in contrast to Eq. (2.12)] does depend on the position of the particle. Therefore, we must calculate the electric field contributed by charge q_c on the grid inside smearing radius R_e and the corresponding self-energy. It can be updated via

$$\psi_{self}^{q_c-new}(\mathbf{r}_i)=\psi_{self}^{q_c-old}(\mathbf{r}_i)+\zeta[\Gamma q_c f_i(\mathbf{r}_c)+\nabla\cdot(P(\mathbf{r}_i)\nabla\psi_{self}^{q_c}(\mathbf{r}_i))]. \tag{2.14}$$

This is similar to Eq. (2.10). But the averaged charge density is replaced by $q_c f_i(\mathbf{r})$. Then the virial for DPD simulation is

$$W_\mu=L_\mu\frac{\partial U}{\partial L_\mu}=\sum_{q_c}\sum_i q_c[\nabla_\mu(\psi(\mathbf{r}_i))-\nabla_\mu(\psi_{self}^{q_c}(\mathbf{r}_i))]f_i(r_c)\mathbf{r}_i^\mu+\sum_{\alpha,\beta>\alpha}\mathbf{F}_{\alpha\beta,\mu}^C\mu_{\alpha\beta}. \tag{2.15}$$

Here L_μ is the box size in μ direction, $\mathbf{r}_i^\mu$ stands for the component μ of the position of node i. $\mathbf{F}_{\alpha,\beta,\mu}^C$ represents the conservative force between particles α and β in the μ direction, $\mu_{\alpha\beta}$ is the μ component of vector $\mathbf{r}_{\alpha\beta}$. The first term in Eq. (2.15) is the virial contributed by the electrostatic interactions; the second is the traditional virial for the pairwise interactions in DPD. By the form of the first term in Eq. (2.15), the electrostatic force on a charge is

$$\mathbf{F}_\mu^{el}(\mathbf{r}_c)=-\sum_i q_c[\nabla_\mu(\psi(\mathbf{r}_i))-\nabla_\mu(\psi_{self}^{q_c}(\mathbf{r}_i))]f_i(\mathbf{r}_c). \tag{2.16}$$

2.4 Constant surface tension and normal pressure ensemble

The constant surface tension and normal pressure ensemble, $N\gamma_s P_\perp T$, is physically well suited to study interfacial systems such as fluid lipid bilayer membranes in water. The surface tension is a macroscopic quantity which is defined as the average of the difference between the normal and tangential pressures multiplied by the dimension of the simulation box in the bilayer normal direction,

$$\gamma_s=\left\langle L_z\times[P_z-0.5(P_x+P_y)]\right\rangle. \tag{2.17}$$

In the $N\gamma_s P_\perp T$ ensemble, constant normal pressure is maintained by adjusting the length of the simulation box along the bilayer normal direction; the surface area is allowed to fluctuate to keep a constant surface tension. Here we employ the Langevin piston approach [22] which is developed by Jakobsen for DPD simulations [23]. In the orthorhombic box, to maintain target pressure, pistons with "mass" Mg in three directions are applied to the box. The Langevin piston approach has the advantage of fast equilibration and short correlation times of various system variables, as detailed in Ref. [23].

3 Results and discussions

3.1 Set of initial configurations

Initially, a tensionless lipid bilayer membrane composed of 1,600 lipids is located on the x-y plane in the middle of our simulation box with size $32r_0 \times 32r_0 \times 32r_0$ ($r_0 \approx 0.8$ nm), as seen in Figs. 1 and 2. 30% of the lipids are negatively charged and distributed randomly on both leaflets of the membrane. The overall bead density is set to $\rho = 3/r_0^3$, and there are 97,535 beads of all types in the box. Lipid counterions and water are distributed in the space unoccupied by the membrane. The lipid bilayer membrane is relaxed for 100,000 time steps (around $4\mu s$) to reach an equilibrium configuration at zero surface tension. Then 32 peptides, i.e. with peptide/lipid (P/L) molar ratio 2:100, and their counterions are placed randomly about 2 nm away from one of leaflets of the membrane (the lower leaflet in Figs. 1 and 2). At the same time, the same amount of water beads are removed randomly from the box so that the total number of beads in the system is unchanged. This structure is chosen as the initial configuration of the studied peptide-membrane systems. In the text, the (initially) peptide-rich leaflet of the bilayer is referred to as the outmost leaflet of a cell membrane, whereas the peptide-poor leaflet is referred to as the inner leaflet of the cell membrane. Periodic boundary conditions are used in all the simulations.

3.2 Effects of force parameters on the mechanism and kinetics of peptide translocation

The physical-chemical properties of peptides, which are represented by the strength of the peptide-lipid interaction and the peptide-water interaction, may influence the mechanism and kinetics of peptide action on the bilayer membrane. Here we will explore these effects systematically, by modifying the corresponding short-range interaction parameters, namely the a-parameters in Eq. (2.2). On the other hand, the long-range electrostatic interactions parameters, i.e., bead charges are held fixed at their values discussed in Section 2.1. We note that the mechanisms of peptide-membrane interaction under various electrostatic conditions have been discussed in detail in our previous paper [18]. The electrostatics plays a threefold role: (1) It helps the positively charged peptides targeted binding onto the surface of negatively charged membranes; (2) The repulsion between the peptides pushes them apart preventing them to aggregate into large domains (clusters) on the membrane surface; (3) The attraction between the peptides and distal membrane surface speeds up the peptide translocations. In the simplified DPD simulations where electrostatic interactions are not included, we have indeed found that the peptides adsorbed on membrane surfaces cluster into large domains. Such tightly bound peptide molecules can only promote the formation of pores composed of only lipid molecules and speed up their flip-flop rate, however the peptide molecules themselves have a lower affinity to translocate across the bilayer. In this article, we focus on realistic charged

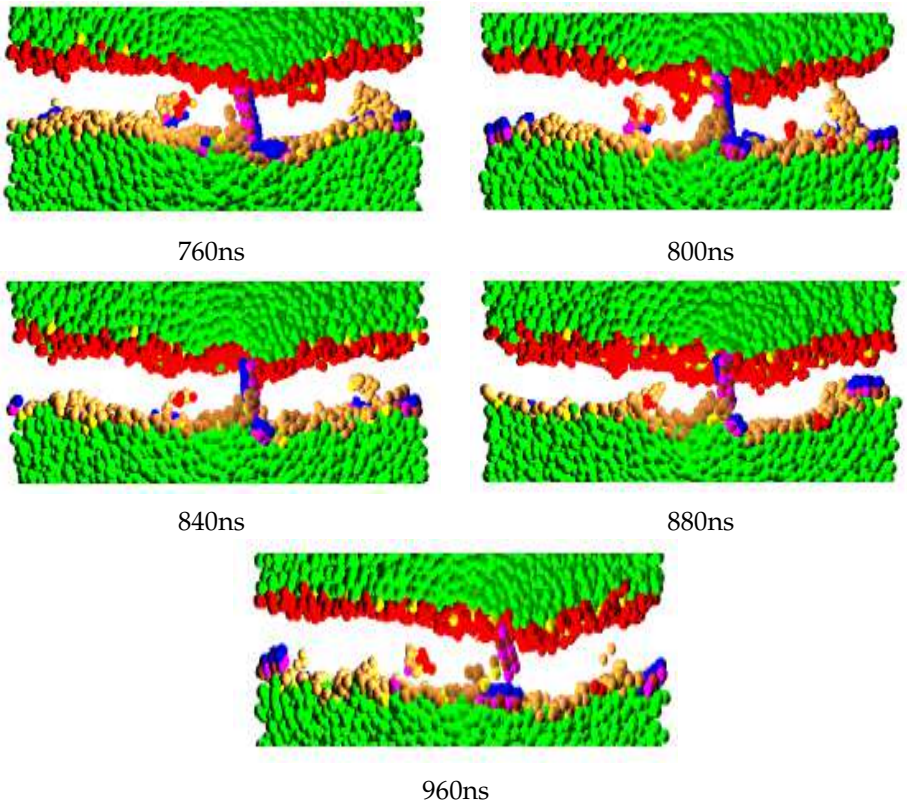

Figure 1: Time sequence of the cross sectional images for peptide translocation across a lipid bilayer membrane with $a_{phc}=35$, at which the intermediate insertion state is a worm-hole like structure composed of a single peptide and a few lipids. For clarity, the tails of lipid molecules are not shown. The neutral head groups of the lipid are in red color on the upper leaflet and in gold in the lower leaflet. Charged head beads of the lipid are yellow. Water beads are in green. The hydrophilic segment of the peptide is in purple and the hydrophobic segment is in blue.

cationic peptide-anionic membrane systems in which peptides do not cluster and may thus have a high affinity to translocate, under the circumstances discussed in the following.

We now proceed to discuss our simulations. First, we have run the simulations in $N\gamma_s P_\perp T$ ensemble by using the same parameter set as in the NVT ensemble in Ref. [18]. Peptide translocation across the membrane via an intermediate hole composed of only one peptide is observed like in the NVT ensemble. The mechanisms of such translocation pathway have been discussed in detail in our paper [18]. It can be briefly described as the following: The binding of the peptide onto the surface of the membrane disrupts the structure of the bilayer by thinning it so that the local tension increases. To relief the induced local tension, the peptide molecule tends to tilt and insert into the membrane core. Next, the electrostatic attraction between the peptide and the acidic lipid heads on the distal (inner) membrane leaflet further promotes the peptide to move toward the other

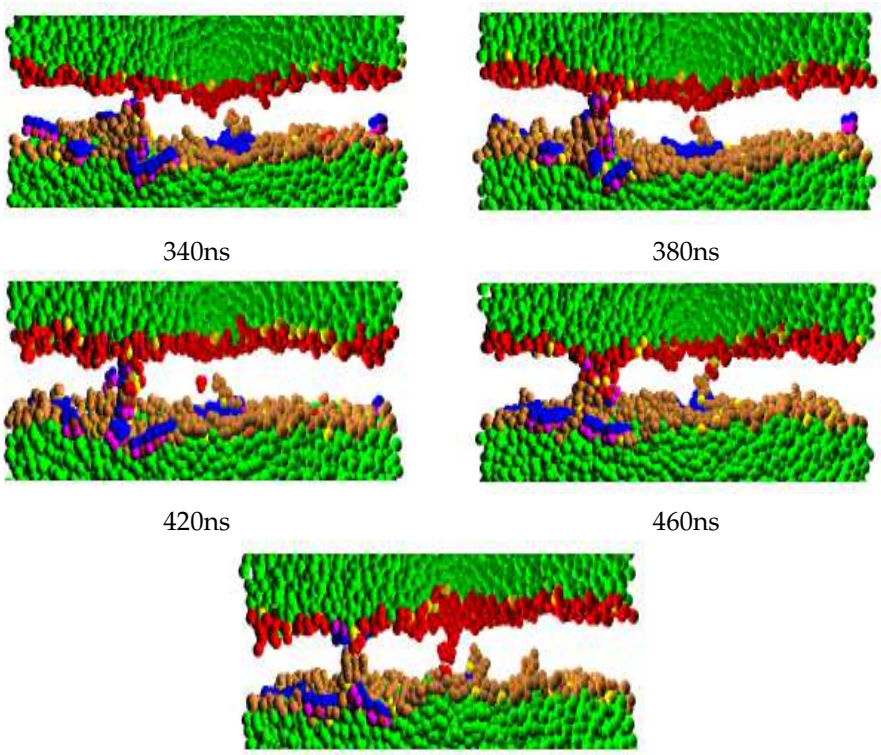

Figure 2: Time sequence of the cross sectional images for peptide translocation across a lipid bilayer membrane with $a_{phc}=50$, at which more lipid molecules are associated with the translocating peptide molecules.

side of the bilayer. In this way, a peptide is capable to translocate across the membrane via a worm-like hole formation.

The kinetics of the peptide translocation can be described as a three-step pathway: initial parallel (to the bilayer) adsorption state on the outmost leaflet of the bilayer, perpendicular insertion state, and a final parallel adsorption state on the inner leaflet of the bilayer. The time sequence of the snapshot for the translocation is given in Fig. 1. (To have a clear view, the system is cut into several slices. Fig. 1 gives the cross sectional images of one of the slices at different times.) Our simulations show that the peptide translocations are stochastic events occurring at random instants of time.

We note that within this parameter set, the peptide has a high affinity to insert into the hydrophobic core of the membrane. It is because the interaction parameter a_{phc} between the hydrophilic part of the peptide and the lipid tail is equal to interaction parameter a_{phw} between peptide and water ($a_{phc}=a_{phw}=35$, [18]). Thus, the free energy needed for the peptide molecule end to intrude into the water is comparable to the free energy needed to insert it into the hydrophobic core of the membrane. Such a weak repulsion between the hydrophilic part of peptide and lipid tail implies that the secondary structure

of the peptide may change when it inserts into the membrane: peptide can easily refold to expose its hydrophobic residues to the lipid tails, i.e., to the hydrophobic core of the bilayer.

These features however are not generic to all peptides. For the peptides tending to maintain their secondary structures after binding with lipid bilayers, the hydrophilic beads of the peptides and the tail beads of lipids should repel each other relatively more strongly. To explore such situations, we consider the case with $a_{phc}=50$ so that the hydrophilic polar part of the peptide cannot insert easily into the hydrophobic core of the bilayer. Five independent samples at P/L molar ratio 2:100 are then simulated. As to be expected, less peptides translocation are observed: translocation events occurred in only three of the five samples up to $10\mu s$. In each of these samples, only one or two peptides managed to cross the membrane. This is much less than for the case with $a_{phc}=35$ where five or more peptides are observed translocated across the membrane in each sample up to $10\mu s$.

The force parameters also affect the conformation of the intermediate insertion state. At $a_{phc}=35$, a single peptide and a few lipids form worm-hole like trans-membrane structure, see Fig. 1. At $a_{phc}=50$, the membrane hole is also occupied by one peptide, however more lipid molecules heads are associated with it, as seen in Fig. 2. These proximal lipid head groups (from the outer, peptide rich leaflet) follow the moving peptide while the distal lipid head groups (from the inner leaflet) move in the opposite direction to reach to the peptide-rich leaflet. Lipid flip-flopping is thus more often at high a_{phc}.

At high a_{phc}, the peptide has a low affinity to translocate across the bilayer. Thus the membrane-peptide complex has to find an alternative way to relief the local stresses induced by the binding of the peptides. Indeed, we find that the peptides accompanied with lipid heads and water self-assemble to form a *hydrophilic core* confined inside the hydrophobic domain of the bilayer membrane. The snapshots of the formation of this novel structure are shown in Fig. 3: In the lower leaflet region with high peptide concentration, both lipid heads and peptides are under local compressional stresses. These stresses relax by a massive intrusion of the peptides accompanied with lipid heads moving together into the hydrophobic membrane center (between the two membrane leaflets). The intrusion grows parallel to the bilayer. The tails of the lipids associated with peptides assume orientations perpendicular to the intrusion, see Fig. 4. Thus a new layer is formed trapped inside the membrane. The new layer has hydrophilic core and a hair comprised of lipid tails, much like the *inner shell* of a *discoidal vesicle*, as seen in the last snapshot of Fig. 3 and in Fig. 4. Here, in contrast to an ordinary vesicle, the outer shell is not closed. Rather, it is continuously connected to the leaflets of the bilayer membrane.

The presence of the hydrophilic core (and the accompanying lipid tails) induces high local curvature deformations on the surrounding lipid bilayer membrane, see Figs. 3, 4, 5 and 6. This effect is prone to eventually rupture the membrane and thus induce cellular leakage promoting bacterial death. Even though no water pore nucleation is observed within our simulation time, lethal cell leakage is possible to occur: In Fig. 4, we give the image of the last snapshot of Fig. 3 with explicit lipid tails. We can see that the lipid

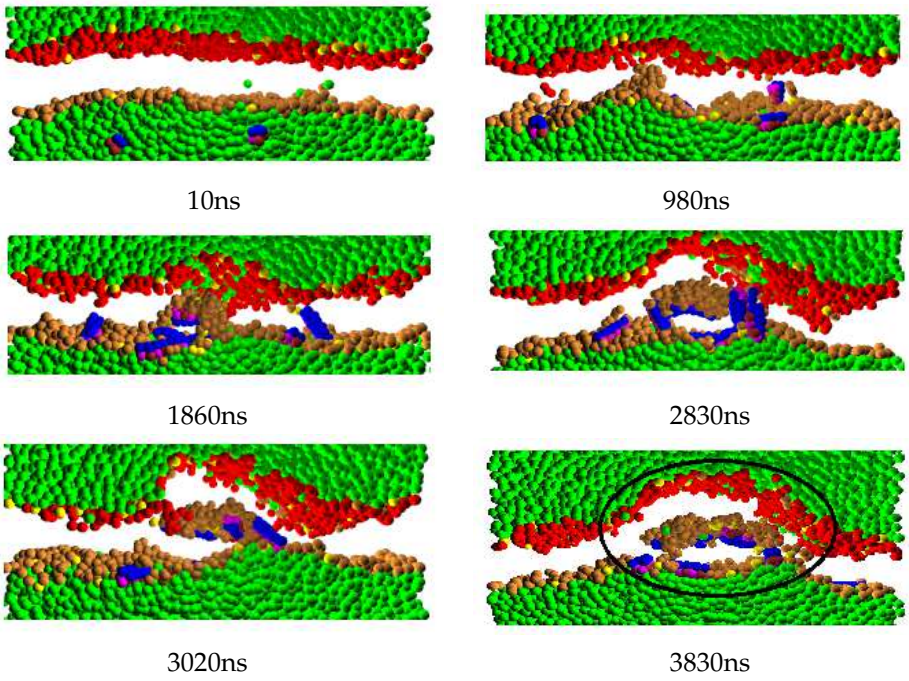

Figure 3: Continuation of Fig. 2. Time sequence of the cross sectional images showing the formation of the vesicle-like structure (hydrophilic core) at $a_{phc}=50$. For clarity, the tails of lipid molecules are not shown.

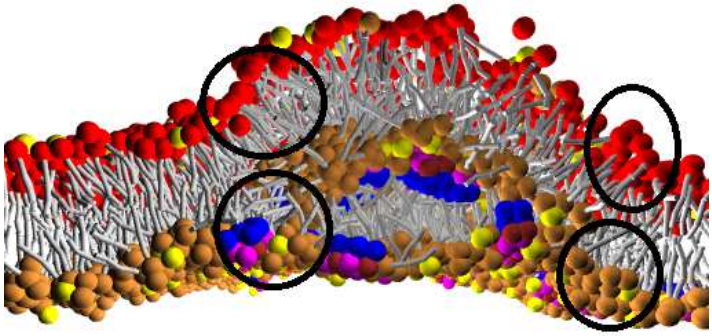

Figure 4: The vesicle-like structure with lipid tails explicitly shown. In the circled regions, tails are highly splayed.

tails are highly splayed along the rim of the outer shell of the vesicle-like structure, as seen in the circled region in Fig. 4. In this region, pore nucleation and/or fracture of individual leaflets are favored. Once this happens, a true vesicle will form, see Fig. 5. Detachment of this discoidal vesicle will leave behind a large hole in the bilayer. Such a membrane disintegration is somewhat similar to that in the pictorial "carpet model" [6]. Yet, our overall picture, involving a vesicle-like structure, is different from the carpet model where trans-membrane and translocated peptides completely surround a part of

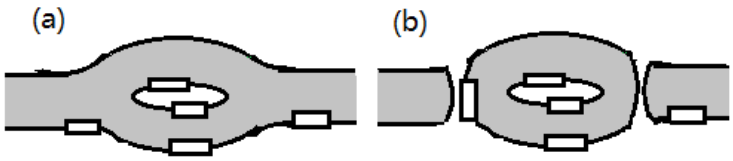

Figure 5: The cartoon of (a) a vesicle-like structure and (b) a true vesicle formation which disintegrates the bilayer membrane. The rectangles represent peptides. The solid lines represent the hydrophilic surfaces of the membrane. The gray shadow is the hydrophobic core of the membrane.

the membrane and induce formation of a micelle (in a detergent like fashion). In contrast to this, we find that peptides can induce formation of vesicle-like structures even at relatively low peptide concentrations. Thus, in particular, the rim of the vesicle as in Fig. 5(b) need not be massively covered by peptides. Indeed, a massive intrusion of lipids complexed with peptides, yielding the formation of the vesicle-like structure, is observed in our simulations at peptide to lipid molar ratios as small as 2:100. Via the here suggested mechanism, we expect antimicrobial peptides can kill bacteria at significantly lower concentrations than expected on the basis of the pictorial carpet model. It is illuminating to note that, on the molecular level, our model does have deep relations to the qualitative carpet model [6]. Indeed, both models rely on the microscopic conditions needed for the peptides to massively associate with lipid heads and stay away from the hydrophobic lipid tails. As discussed here, this condition is met by increasing the strength of the repulsion between the hydrophilic peptide molecule portion and hydrophobic lipid tails, encoded in the interaction parameter a_{phc}. The simulations presented here show that this microscopic interaction plays the dominant role in controlling the large scale structures involved in membrane disintegration. Indeed, as the a_{phc} increases, the size and the occurrence frequency of the vesicle-like structures are also observed to increase. This parameter thus plays a prominent role.

We note that another property that may potentially affect the mechanism of activity of the peptides is their hydrophobicity. Yet, by changing the corresponding force parameter a_{pcw} from 120 to 200 and 300, we did not observe any qualitatively significant effects comparable to those obtained by changing the parameter a_{phc}. Interestingly however, another parameter, the a_{phh} (the repulsion parameter between the hydrophilic peptide portion and lipid heads), can substantially affect the mechanism of the peptide activities. We find that reducing the a_{phh} produces similar effects (hydrophilic core formation) as increasing the a_{phc}. For example, by reducing a_{phh} to 10 and 15, hydrophilic core formations are observed within 1 and 2 microseconds, respectively, even at $a_{phc}=35$, as shown in Fig. 7 (for $a_{phh}=15$). On the other side, for $a_{phh}=35$, no hydrophilic core was observed at $a_{phc}=35$. Thus, reducing the repulsion (or increasing effective attraction) between the hydrophilic portions of the peptide and lipid heads also enhances the peptide-lipid association and thus favors the formation of vesicle-like structures, i.e., hydrophilic cores confined within the membrane.

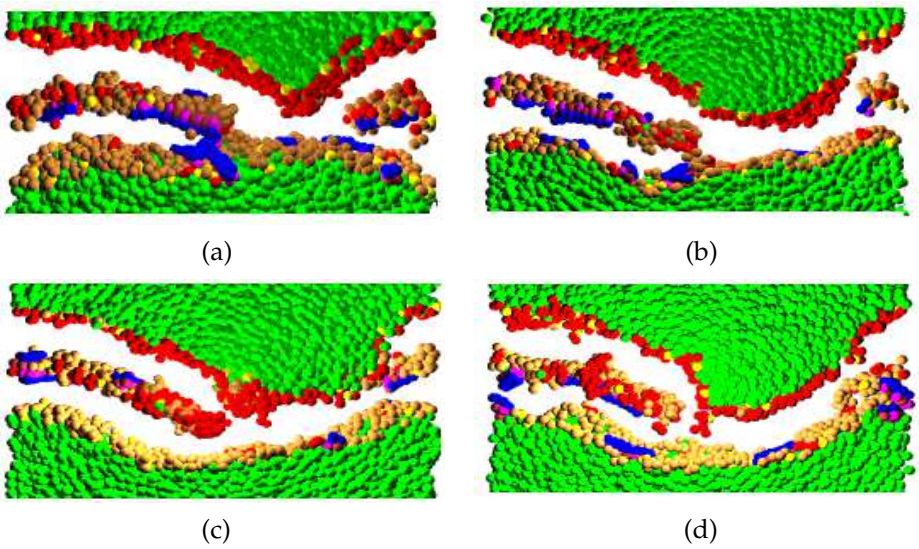

Figure 6: A late simulation time ($t=10$ microseconds) view of the buckled membrane structure formed at $a_{phc}=50$. To have a complete view, four slices, (a), (b), (c), and (d), are cut out of the system, and the figure gives the images of all these slices. For clarity, the tails of lipid molecules are not shown. We note that significant membrane buckling develops already at earlier times [see Fig. 3].

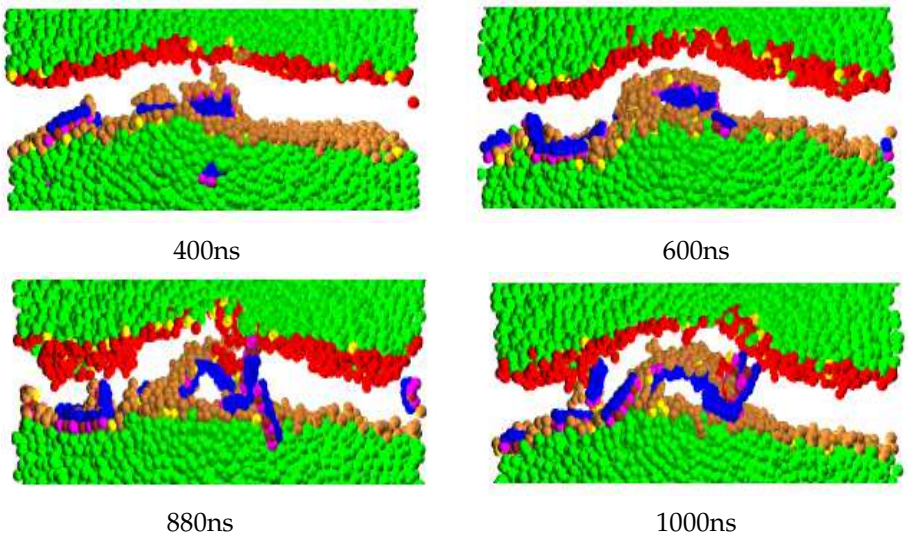

Figure 7: Time sequence of the cross sectional images for the formation of the vesicle-like structure (hydrophilic core) at $a_{phc}=35$ and $a_{phh}=10$.

From Figs. 3, 6 and 7, we can see that the presence of the hydrophilic core induces strong curvature and buckles the surface of the membrane. This buckled membrane phase is very stable. We did not observe the disappearance of the hydrophilic core in

the reachable time scale (up to $10\mu s$). The rim of the core occasionally touches the lower monolayer of the membrane to accumulate more lipids and peptides, and upper monolayer to release or exchange lipids. The size of the core increases with time and a multilayered corrugated structure is formed. In Fig. 6, we display this buckled membrane structure by giving several slices of our system at the late simulation time of 10 microseconds. At this time scale, the core size has reached more than half of our system lateral size. The most striking feature of our membrane structure in Fig. 6 is its highly buckled morphology. These theoretical results support very recent experimental observation of Fantner *et al.* [27], that the addition of antimicrobial peptides changes the surface of the bacteria from smooth to corrugated, during the incubation stage in which the steadily evolving corrugated membrane state develops.

The lesion caused by the buckling of the membrane may not be itself sufficient to lead to microbial death [27]. The death ("execution") of the bacteria should be related to the membrane permeability, as discussed in Section 3.3 below. We also note that the lipids composing the hydrophilic core are mainly from the outmost leaflet of the bilayer. It means the distribution of the lipids between the leaflets of the bilayer is locally scrambled. Such scrambling may destroy the trans-membrane potential and cause partial loss of the viability of the cell.

3.3 Permeability of the membrane

When a peptide molecule transports across the bilayer, the redistribution of the water and lipids associated with the peptide is also observed. We found that at the low $a_{phc}=35$ (the simulation in Fig. 1), the peptide mediated membrane pores are poorly permeable to water, whereas lipid flip-flops are infrequent: Less than 5 flip-flops take place (in each of the five samples) from the peptide-rich outer membrane leaflet to the peptide-poor inner leaflet, within $10\mu s$. In the opposite direction, flip-flops were not observed within the time limits of our simulations. Yet, peptide translocations are observed even with such non-permeable membrane holes, so the translocated peptides can pass onto the surface of the inner leaflet. This corresponds to the microbial killing mechanism in which the transported peptide eventually reaches the cell cytoplasm and affects the cytoplasmic membrane septum formation, or inhibits the synthesis of cell-wall, nucleic-acids and proteins [4].

On the other hand, at the high $a_{phc}=50$ (the simulation in Figs. 2 and 3), more than 10 lipid flip-flops in both directions are regularly observed (in each of the five samples) within $10\mu s$, yet water permeability remains small. Interestingly, we find that increasing hydrophilicity of peptide does not significantly affect the water permeability, as we evidenced by doing simulations in which we reduced the parameter a_{phw} from 35 down to 15 and 25. Yet, this change did not affect the permeability much.

However, at high a_{phc}, the peptides buckle the membrane by forming vesicle-like structures, and extensive leakage of the cell is possible, as discussed in Section 3.2. The nucleation of such a water pore is not observed so far within our available simulation

time. The pore nucleation time is thus certainly longer than our simulation time ($\sim$ ten microseconds). In fact, longer nucleation times for water pores are in accord with recent experiments [27] showing that a swift execution of bacteria is actually *postponed* by a long incubation stage (with time scale measured in minutes) over which the bacteria are likely still alive (thus, water pores not yet formed), while their membranes corrugate, i.e., undergo buckling deformation. This is in agreement with our simulations of the buckled membrane state evolution in Fig. 3 and in Fig. 6. Indeed, the kinetics of the AmPs activity measured by atomic force microscopy indicates that the buckled membrane phase is a long lived incubation phase [27].

4 Conclusions

Physical understanding of the mechanisms employed by antimicrobial peptide to kill bacteria is only beginning to emerge. It is hoped it may help in designing new non-viral peptide based drugs. Coarse-grained Dissipative Particle Dynamics simulations with large temporal and spacial scales permit us to gain deeper insights into the bacteria killing mechanisms. We found that the strength of the interactions between the peptide and the lipid determines the character of this mechanism. The peptides can destroy vital functions of the affected cell either by translocating across the bilayer and accumulating in the inner cytoplasm, or by forming vesicle-like structures disintegrating the membrane. The simulations presented here elucidate which microscopic interactions play the dominant role in controlling the large scale structures involved in membrane disintegration.

We have revealed that the strength of the interactions between the peptide and the lipid, which governs the various folding structures of the peptides in the adsorption states and insertion states, plays a prominent role. If in the insertion state the peptides refold to expose their hydrophobic residues to the membrane core, the peptides can kill bacteria by translocating across the bilayer and accumulating in the inner cytoplasm. On the other side, if in the insertion state the peptides retain their secondary structures, the peptides can disintegrate the membrane by associating with lipid heads and forming hydrophilic plate-like cores confined inside the membrane core. These hydrophilic cores are stable, they corrugate the membranes, and they induce strong curvature effects that may rupture membranes. The hydrophilic core model introduced by us here can well explain both the membrane buckling and the time lag between incubation phase and execution phase seen in recent experiments with antimicrobial peptides.

Acknowledgments

This work is supported by National Science Foundation of China (Grant No. 20873007). We are thankful to the referee for very useful comments.

References

[1] B. Alberts, A. Johnson, J. Lewis, M. Raff, K. Roberts, and P. Walter, Molecular Biology of Cell, Garland Science, New York, 2002.

[2] T. H. Denmark, Themed issue: Membrane biophysics, Soft Matt., 5 (2009), pp. 3145- 3147.

[3] M. Zasloff, Antimicrobial peptides of multicellular organisms, Nature (London, United Kingdom), 415 (2002), pp. 389-395.

[4] K. A. Brogden, Antimicrobial peptides: Pore formers or metabolic inhibitors in bacteria? Nat. Rev. Microbiol., 3 (2005), pp. 238-250.

[5] K. Matsuzaki, Why and how are peptide-lipid interactions utilized for self-defense? Magainins and tachyplesins as archetypes, Biochim. Biophys. Acta., 1462 (1999), pp. 1-10.

[6] Y. Shai, Mechanism of the binding, insertion and destabilization of phospholipid bilayer membranes by α-helical antimicrobial and cell non-selective membrane-lytic peptides, Biochim. Biophys. Acta., 1462 (1999), pp. 55-70.

[7] L. Yang, T. M. Weiss, R. I. Lehrer, and H. W. Huang, Crystalization of antimicrobial pores in membranes: Magainin and protegrin, Biophys. J., 79 (2000), pp. 2002-2009.

[8] P. La Rocca, P. C. Biggin, and D. P. Tieleman, Simulation studies of the interaction of antimicrobial peptides and lipid bilayers, Biochim. Biophys. Acta., 1462 (1999), pp. 185-200.

[9] J. H. Lin and A. Baumgaertner, Stability of a melittin pore in a lipid bilayer: A molecular dynamics study, Biophys. J., 78 (2000), pp. 1714-1724.

[10] H. Leontiadou, A. E. Mark, and S. J. Marrink, Antimicrobial peptide in action, J. Am. Chem. Soc., 128 (2006), pp. 12156-12161.

[11] H. D. Herce and A. E. Garcia, Molecular dynamics simulations suggest a mechanism for translocation of the HIV-1 Tat peptide across lipid membranes, Proc. Natl. Acad. Sci. U. S. A., 104 (2007), pp. 20805-20810.

[12] F. Jean-Francois, J. Elezgaray, P. Berson, P. Vacher, and E. J. Duforc, Pore formation induced by an antimicrobial peptide: Electrostatic effects, Biophys. J., 95 (2008), pp. 5748-5756.

[13] C. F. Lopez, S. O. Nielsen, P. B. Moore, and M. L. Klein, Understanding nature's design for ananosyringe, Proc. Natl. Acad. Sci. U. S. A., 101 (2004), pp. 4431-4434.

[14] C. F. Lopez, S. O. Nielsen, P. B. Moore, and M. L. Klein, Structure and dynamics of model pore insertion into a membrane, Biophys. J., 88 (2005), pp. 3083-3094.

[15] C. F. Lopez, S. O. Nielsen, G. Srinivas, W. F. DeGrado, and M. L. Klein, Probing membrane insertion activity of antimicrobial polymers via coarse-grain molecular dynamics, J. Chem. Theor. Comput., 2 (2006), pp. 649-655.

[16] M. Venturoli, B. Smit, and M. M. Sperotto, Simulation studies of protein-induced bilayer deformations, and lipid-induced protein tilting, on a mesoscopic model for lipid bilayers with embedded proteins, Biophys. J., 88 (2005), pp. 1778-1798.

[17] G. Illya, and M. Deserno, Coarse-grained simulation studies of peptide-induced pore formation, Biophys. J., 95 (2008), pp. 4163-4173.

[18] L. Gao and W. Fang, Effects of induced tension and electrostatic interactions on the mechanisms of antimicrobial peptide translocation across lipid bilayer, Soft Matt., 5 (2009), pp. 3312-3318.

[19] P. Espanol and P. B. Warren, Statistical mechanics of dissipative particle dynamics, Europhys. Lett., 30 (1995), pp. 191-196.

[20] R. D. Groot and P. B. Warren, Dissipative particle dynamics: Bridging the gap between atomistic and mesoscopic simulation, J. Chem. Phys., 107 (1997), pp. 4423-4435.

[21] R. D. Groot and K. L. Rabone, Mesoscopic simulation of cell membrane damage, morphol-

ogy change and rupture by nonionic surfactants, Biophys. J., 81 (2001), pp. 725-736.
[22] G. J. Martyna, D. J. Tobias, and M. L. Klein, Constant pressure molecular dynamics algorithms, J. Chem. Phys., 101 (1994), pp. 4177-4189.
[23] A. F. Jakobsen, Constant-pressure and constant-surface tension simulations in dissipative particle dynamics, J. Chem. Phys., 122 (2005), pp. 124901.
[24] R. D. Groot, Electrostatic interactions in dissipative particle dynamics-simulation of polyelectrolytes and anionic surfactants, J. Chem. Phys., 118 (2003), pp. 11265-11277.
[25] P. H. Hunenberger, Calculation of the group-based pressure in molecular simulations. I. A general formulation including Ewald and particle-particle-particle-mesh electrostatics, J. Chem. Phys., 116 (2002), pp. 6880-6897.
[26] L. Gao and W. Fang, Communications: Self-energy and corresponding virial contribution of electrostatic interactions in dissipative particle dynamics: Simulations of cationic lipid bilayers, J. Chem. Phys., 132 (2010), pp. 031102-031104.
[27] G. E. Fantner, R. J. Barbero, D. S. Gray and A. M. Belcher, Kinetics of antimicrobial peptide activity measured on individual bacterial cells using high-speed atomic force microscopy, Nat. Nanotech., 5 (2010), pp. 280-285.